Dual-Doppler Lidar Measurement of Winds in the JAWS Experiment

JEFFRY ROTHERMEL*

Atmospheric Sciences Division, NASA/Marshall Space Flight Center, Huntsville, AL 35812

CATHY KESSINGER

*National Center for Atmospheric Research,** Boulder, CO 80307*

DARIEN L. DAVIS†

NOAA/ERL, Wave Propagation Laboratory, Boulder, CO 80307

(Manuscript received 24 February 1984, in final form 22 October 1984)

ABSTRACT

Two 10.6 μm coherent Doppler lidars participated in the Joint Airport Weather Studies (JAWS) Project field experiment, conducted in summer 1982 near Denver's Stapleton International Airport. One was operated by NOAA/ERL, Wave Propagation Laboratory (WPL), the other by NASA, Marshall Space Flight Center (MSFC). Periodic coordinated scans were made with the two lidars spaced 15 km apart. This permitted the calculation of Cartesian winds. This paper presents 1) a brief comparison of radar and lidar system and performance characteristics, 2) results of the first dual-Doppler analyses to be based upon lidar measurements and 3) a comparison of radial wind estimates between the MSFC lidar and a 5.5 cm Doppler radar operated by the National Center for Atmospheric Research (NCAR).

Dual-Doppler analyses were made for the flow behind gust fronts, with the desired flow fields consistent with both surface winds measured by the NCAR Portable Automated Mesonet (PAM) and models derived from previous studies of Great Plains thunderstorm outflows. A comparison of low elevation scans made by the MSFC lidar and the NCAR CP-4 Doppler radar revealed distinct differences which could be explained by a bias in the radar estimates (toward weaker velocities) due to ground clutter contamination. Root-mean-square (rms) difference between radar- and lidar-measured radial velocities was 3.1 m s^{-1} which could be explained by other causes; however, the mean of the radar data set was 1–2 m s^{-1} lower than that of the lidar. These findings are consistent with a recent previous study comparing the WPL lidar with the NCAR CP-3 5.5 cm radar.

1. Introduction

The Joint Airport Weather Studies (JAWS) Project conducted a field experiment near Denver's Stapleton International Airport during the summer of 1982. The principal objective of JAWS was to study convectively driven downdrafts and resulting outflows near the surface. A description of the JAWS Project scientific objectives and applications has been provided by McCarthy *et al.* (1982). Facilities included 5.5 cm (CP-3 and CP-4) and 10.7 cm (CP-2) Doppler radars operated by the National Center for Atmospheric Research (NCAR), as well as a network of 27 NCAR Portable Automated Mesonet (PAM) stations. Each PAM station included an anemometer mounted at a height of 4 m; average station separation was 4 km. Data were sampled at 1-second intervals and a 1-minute average was computed and recorded on the minute. A list of the organizations and equipment that participated in JAWS is given by McCarthy *et al.* (1983).

The JAWS Project was marked by the participation of two ground-based, CO_2-pulsed Doppler lidars, one operated by NOAA/ERL, Wave Propagation Laboratory (WPL) and the other by NASA, Marshall Space Flight Center (MSFC). Periodic coordinated scans were made with the lidars spaced 15 km apart, which permitted the calculation of Cartesian wind fields. This paper presents results of the first dual-Doppler analyses using lidar measurements. Although the primary intention is to demonstrate that a dual-Doppler lidar analysis is feasible, brief consideration is given to how the results compare with previous studies of thunderstorm outflows. A comparison of radial velocity estimates between the MSFC lidar and the NCAR CP-4 radar is described. Figure 1 shows the location of the lidars, radars, and PAM stations.

* Universities Space Research Association Visiting Scientist.
** NCAR is sponsored by the National Science Foundation.
† Present affiliation: Program for Regional Observing and Forecasting Services, NOAA/ERL, Boulder, CO.

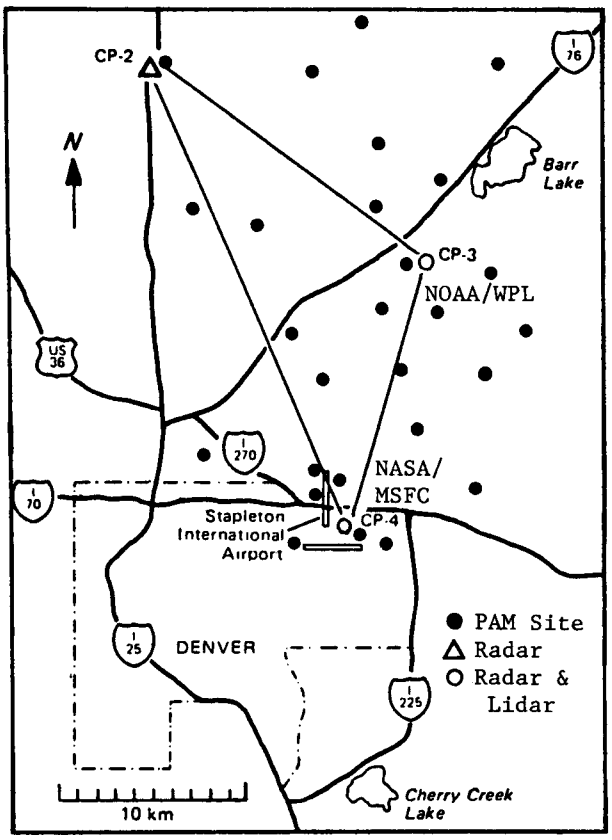

FIG. 1. Location of lidars, radars and Portable Automated Mesonet (PAM) stations during the Joint Airport Weather Studies (JAWS) Project field experiment, summer 1982.

2. Description of lidar systems

The purpose of this section is to describe briefly the two lidar systems, since both have come into existence relatively recently. No attempt is made to describe a typical radar operating system, as this has been thoroughly described over the years. Table 1 summarizes system and performance characteristics of the lidars. Both lidars consist of a transmitter, telescope (analogous to the radar antenna), receiver and processor. The WPL system[1] uses a transverse-excited (TE), CO_2 laser as the transmitter. Since TE lasers typically produce pulses with bandwidth on the order of 3 GHz, frequency stability is maintained through insertion of a continuous-wave (CW) low-pressure laser into the TE laser cavity. Radiation from the CW tube "seeds" the TE laser output so that the initial transmit frequency is identical to the CW laser frequency. However, the frequency stabilization is not complete; once lasing occurs the transmit frequency chirps because free electron and gas dynamic effects alter the cavity refractive index. The lidar receiver employs a superheterodyne arrangement. By means of a local oscillator laser, the received signal is optically heterodyned to an intermediate frequency and mixed with signals from a reference oscillator. The resulting in-phase and quadrature signals at baseband are digitized and stored for later analysis. With the exception of the laser type and signal processing algorithm, the bulk of the WPL system is similar to the MSFC system, described later. Additional information on the WPL system may be found in Hardesty *et al.* (1983) and Post *et al.* (1981).

The MSFC lidar system is arranged in a master oscillator, power amplifier (MOPA) configuration. A small portion of the output of the master laser is initially picked off and used in a frequency stabilization loop for the master laser and in an offset locking loop used to maintain a local oscillator at a constant offset frequency from the master laser. The remainder of the output of the master laser is directed to an electro-optic modulator, which amplitude modulates the horizontally polarized beam to form a pulse train. The pulse train passes through a power amplifier, a Brewster window, and again into a quarter waveplate and into the telescope where it is expanded, collimated and transmitted into the atmosphere as a circularly polarized pulse. Each lidar system is contained within a semitractor trailer, the beam being directed through the roof and to a hemisphere scanner. The radiation which is scattered back along the axis of transmission has its sense of polarization reversed (RHC to LHC) and has been Doppler shifted. The backscattered radiation is collected by the telescope and transmitted through the quarter waveplate in the reverse direction where the output is vertically polarized. The return radiation is then reflected off the Brewster window (due to the vertical polarization) and combined with the local oscillator beam. In both systems the return beam is then imaged on a HgCdTe detector that is cryogenically cooled. The frequency of the detector output is the result of a time-varying interference pattern caused by the difference in frequency (i.e. the Doppler shift) between the return beam and the local oscillator. Conceptually, a Fourier analysis of the detector output would yield an amplitude spectrum (Doppler spectrum) of the return signal which in turn is related to the velocity distribution (in a statistical sense) of the aerosols within the illuminated volume. Since the aerosols are assumed to reliably follow the wind, the spectrum could be interpreted as a wind velocity distribution function. In practice only three spectral parameters instead of the entire distribution are obtained through the use of a poly-pulse-pair estimation technique (Lee and Lee, 1980) in the

[1] The present description applies to the configuration during the JAWS experiment. Since then, several modifications have been made.

TABLE 1. Comparison of system characteristics among NASA/MSFC and NOAA/WPL lidars and CP-4 radar.

Characteristic	MSFC lidar	WPL lidar*	NCAR CP-4 radar**
Wavelength (m)	10.6×10^{-6}	10.6×10^{-6}	5.49×10^{-2}
Pulse duration (μs)	2	2	1
Average power (W)	1.7	1	200
Peak power (kW)	7.5	50	200–400
Pulse repetition frequency (Hz)	110	10	500–2000
Number of pulses per velocity measurement	50	1	32–128
Antenna (telescope) diameter (m)	0.31	0.28	3.66
Telescope (antenna) type	off-axis paraboloid	off-axis paraboloid	on-axis paraboloid
Beamwidth (deg)	5×10^{-3}	5×10^{-3}	1.09
Beam diameter at 10 km (m)	0.9	0.9	190
Range resolution (m)	320	500	150
Maximum range (km)			
clear air target	12	17	20–100†
precipitation target	?	22	300
Convective cloud penetration	no	no	yes

* Source: Hardesty *et al.* (1983).
** Equipment specification taken from JAWS Project Operations Summary 1982, February 1983 (NCAR and University of Chicago).
† Representative of summer boundary layer.

MSFC system and the pulse-pair estimation technique for the velocity distribution in the WPL system. These estimations are unbiased in the presence of white noise. For the pulse-pair estimation technique it can be shown that the errors in estimation of the first moment (frequency) for differing lags are independent at low signal-to-noise ratio (SNR). The poly-pulse-pair algorithm exploits this error independence and makes estimates at several lags which are then averaged to provide a final velocity estimate that has a lower error than any of the individual estimates. Both estimation techniques produce the peak intensity, mean frequency shift and frequency spread (spectral width) of the return Doppler spectrum for each resolution element averaged over a selectable number of pulses. The peak intensity provides a relative measure of aerosol density. The mean frequency shift is, of course, used to derive an average value of the line-of-sight wind velocity over the Doppler pulse length.

Similar error sources were present in both lidar systems. Drift in the local oscillator could produce biases as great as 1 m s^{-1}. This offset was a function of time and, in some measurement sets (e.g., that used in the lidar–radar comparison), was negligible. Both hemispheric scanners were accurate to within 1 deg in azimuth and elevation; each trailer was leveled with an accuracy of better than 1 deg. The rms uncertainty in the signal processors was, of course, a function of SNR at weak signal-to-noise ratios. The poly-pulse-pair estimation technique (MSFC system) contained an rms uncertainty of 0.25 m s^{-1} for wideband SNR of 0 dB or greater; the pulse-pair estimation technique (WPL system) contained an rms uncertainty of less than 1 m s^{-1}. The error due to the chirp in the WPL TE laser, which is a function of SNR, is typically less than 1 m s^{-1}.

3. Comparison of radar and lidar characteristics

It is appropriate to describe what the lidar and radar "see." The radar depends upon the presence of at least one of three principal sources of return, two of which are associated with clear air. One source, precipitation, can provide returns within convective systems. The sources of clear air return have been found to vary with wavelength. For moderately sensitive C-band and X-band radars the particulate scatterers in most cases appear to be insects and, less frequently, birds (for a brief discussion of the wavelength dependence phenomenon, see, e.g., Wilson *et al.*, 1980). At wavelengths larger than or equal to 10 cm, the dominant scattering mechanism appears to result from refractive inhomogeneities in the atmosphere. In the planetary boundary layer these inhomogeneities result primarily from water vapor gradients. At higher altitudes, where vapor pressures are low, the greater contribution comes from large temperature gradients. Wilson *et al.* (1980) report routine detection of clear air echoes with the NCAR 5 cm radars during all nonwinter experiments. Doviak and Jobson (1979) successfully used a pair of 10 cm Doppler radars to synthesize three-dimensional kinematic structure in the summer clear air boundary in Oklahoma. An advantage of the lidar is that it relies upon the presence of naturally occurring aerosols, primarily in the diameter range of 1–5 μm. The aerosols within this size range may be assumed to be suspended in the air and advected by the mean wind, eliminating the need to correct for fall velocities. These properties

suggest that in regions, for example, above the boundary layer in clear air, the lidar would be the instrument of choice. In fact, the MSFC lidar has already been used in such a manner in a 1981 flight program which included participation in the Cooperative Convective Precipitation Experiment (CCOPE) (Bilbro *et al.*, 1984). Analysis of the data is still in progress.

Table 1 summarizes system and performance characteristics of the NCAR CP-4 radar, along with those of the lidars. It is apparent from the beamwidths that the lidar can provide much finer transverse resolution; furthermore, errors due to sidelobe contamination are absent. These characteristics allow the lidar to scan arbitrarily close to the surface without susceptibility to ground clutter contamination. It is also noted that the aspect ratio of the scattering volume for the lidar is roughly two orders of magnitude larger than that for the radar scattering. Disadvantages of the lidar are limited range (typically 10–20 km), attenuation by water vapor (10.6 μm is within the water vapor absorption continuum) and scattering within clouds. While cirrus and thin cloud layers can be penetrated and, in some cases, returns obtained from the forward edge of cumulus and rain shafts, the lidar cannot probe within convective clouds or precipitation regions.

The aerosols that produce the lidar signal return are widely dispersed, plentiful in the troposphere and small enough so that their fall speeds are negligible. In contrast, the clear air scatterers for microwave frequencies may not be widely dispersed. For example, index of refraction perturbations may be concentrated on inversions or on the edges of convective structures (see, for example, Hardy and Ottersten, 1969). Furthermore, insects, which may be the primary return for spring and summer C-band and X-band observations, may be concentrated along convergence lines (Wilson *et al.*, 1980). Numerous investigators have mapped the wind field by examining returns from slow flying insects. Uncertainty arising from the motion of insects has been noted in the literature, particularly by Fowler and LaGrone (1969), who showed that some insects can fly at substantial speeds; in one case, maximum speeds of up to 8 m s^{-1} were found. Flight speeds of birds of about 10–20 m s^{-1} have been reported by Eastwood (1967). When taken together with the large beam divergence angle (order of 1 deg), the nonuniformity of distribution of targets, as well as their possible substantial motion (for the case of insects), leads to an average value that may not be representative of the air motion.

4. Method of analysis

Analyses were performed only after eliminating obvious errors due to low SNR (radar and lidar data) and ground clutter (radar data) using the NCAR interactive Doppler Editing Software (IDES) developed at the Field Observing Facility (Oye and Carbone, 1981). To generate Cartesian wind fields from the lidar radial wind measurements, an objective analysis scheme developed at the National Severe Storms Laboratory (NSSL) and described by Ray *et al.* (1980) was used (scheme "A" by their nomenclature). The radial velocity components for each lidar were first interpolated, using a Cressman (1959) weighting function, to a Cartesian grid with horizontal and vertical increments of 0.5 km and overall size 14.5 $\times$ 14.5 $\times$ 1.5 km. To solve for the horizontal wind components u and v [using their Eq. (5)], an initial estimate of w was applied, then upward integration of the anelastic mass continuity equation [their Eq. (4)] gave a refined w, and u and v were recomputed. This procedure was repeated until the solution converged. Vertical velocity was required to vanish at the surface. Because the analyses were done in clear air, the terminal fallspeeds were assumed to be zero. Due to a lack of knowledge of a kinematic upper boundary condition for w, a more sophisticated scheme (i.e., one in which a physical constraint is imposed) was not applied.

Ray *et al.* (1978) have performed an error analysis for horizontal wind fields for multiple radars. In terms of the present study their most relevant finding was that, for the case of two radars (or lidars), upward integration over very shallow depths (in the present study, 1.5 km and less) does not lead to significant error accumulation.

The time variation of the wind field during the period of the measurement set (less than 3 minutes) is a possible error source. Given a windspeed of 15 m s^{-1}, the airflow would travel 3 km or less. However, PAM measurements revealed only minor variations in the flow field over periods of at least 4 min and longer. Therefore, errors from this source are considered to be minor. Other errors conceivably could have been introduced by inhomogeneities in the distribution of aerosols within the scattering volume. In general this error source is not well understood at present; efforts are under way at the Marshall Space Flight Center which will address this problem.

5. Results and discussion

a. 6 August dual analyses

The initial investigation of the coordinated lidar measurement sets focused on 6 August 1982. During the early evening hours a squall line moved through the JAWS network from the north, preceded by a large gust front that weakened as it moved through the network. The front, which produced roughly a 3 K drop, passed the WPL lidar at 1945 (all times are MDT) and the MSFC lidar at 2007 with speed 11 m s^{-1} toward 205 deg. The precipitation area was located

~15 km north of the front when it entered the PAM network at ~1920. Returns from CP-4 (see Fig. 2) showed only a narrow band of velocities (maximum ~13 m s^{-1}), which could be explained in part by a sharp gradient of average refractive index associated with thermal and moisture gradients across the front (Atlas, 1964). The dominant scatterers, however, were probably slow flying insects with, perhaps, insectivorous birds (Harper, 1958), which were concentrated in the convergence zone ahead of the cold air outflow (Wilson *et al.*, 1980). Behind the front the radar reflectivities were ~ −20 dBZ and velocities ~ 0, reflecting the loss of usable scatterers. As the gust front continued to move through the JAWS network, this pattern in the radar observations persisted, even though the WPL lidar and the PAM stations were indicating significant velocities behind the front. From 2012 onward, however, CP-4 began obtaining returns out to ~12 km which were more consistent with those indicated by the two lidars. A comparison of the radial velocity measurements made between CP-4 and the MSFC lidar is described in Section 5c.

Two dual Doppler lidar analyses were made from scans at 2016 and 2020 and which extend from 1 to 5 deg elevation. The common volumes were within the cold air outflow, well after the gust front had passed the MSFC lidar. Unfortunately, insufficient data were taken to calculate the Cartesian winds while the front was between the lidars. Figure 3 shows the 3 min averaged wind field as measured by the PAM network from 2015 to 2017, superimposed on the lowest horizontal level of the first dual Doppler analysis (2016). The analysis at this level was based upon radial velocity estimates interpolated to a horizontal grid of height 0.0 km using the Cressman weighting function. The circle and triangle mark the locations of the MSFC and WPL lidars, respectively. Over most of the JAWS network the flow field as measured by PAM was nearly uniform, with weakly divergent flow in the southwestern quadrant. In general the derived wind vectors agree with the PAM wind directions to within 30 deg and typically less. The PAM wind speeds are weaker (by a factor of almost one-half) because the flow near the surface is retarded by frictional drag (Goff, 1976). Concomitant deviations in wind direction could be explained by the elevation of the lidar beams above the surface (several hundred meters) within an Ekman boundary layer. At 0.5 km the lidar-derived horizontal wind speeds ranged from 8 to 15 m s^{-1}, with virtually no change in direction from the surface winds. At 1.0 km, speeds varied from 7 to 12 m s^{-1}, and there was less directional uniformity. By 2020 the gust front was ~8 km south of the MSFC lidar with no rain being reported between the lidars. Since dual analyses using lidar data heretofore had not been made, and since additional data were available, a second dual analysis was warranted to help determine whether the agreement between the first analysis and the PAM winds was fortuitous. Figure 4 shows the 3 min averaged wind field as measured by the PAM network from 2019 to 2021, superimposed on the second dual Doppler analysis. Similar agreement was found between the observed and derived wind directions. Although a few individual wind vectors differ directionally by as much as 30 deg, generally the two lidar-derived surface flow fields agree closely. Divergence in the southwestern quadrant was again diagnosed. Excellent agreement at the two times was found for the horizontal motion fields at higher levels.

Although it is the primary intention to demonstrate that a dual Doppler lidar analysis is feasible, it is also

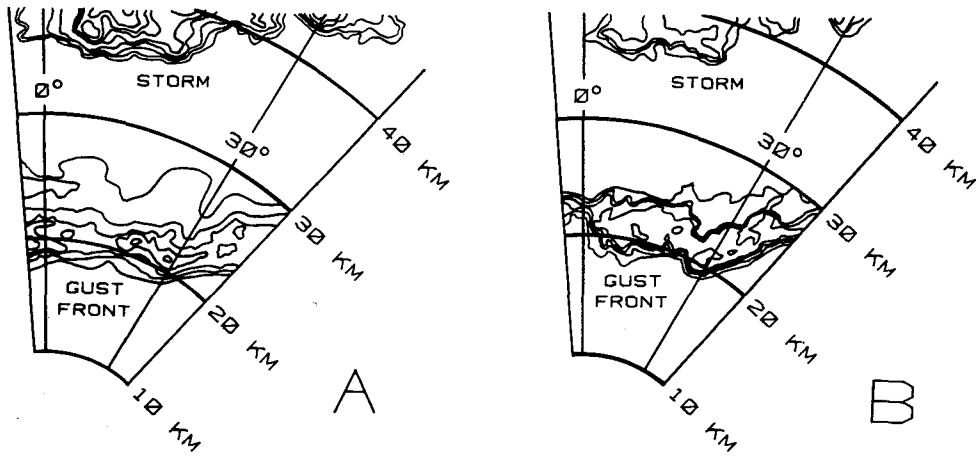

FIG. 2. Plan views of CP-4 radar data measured at 1939 MDT, 6 August 1982 at 1.2 deg elevation: (a) contours of radar reflectivity beginning at −20 dBZ and contoured in 4 dBZ steps; (b) contours of radial velocity beginning at −1 m s^{-1} and contoured in −2.5 m s^{-1} steps.

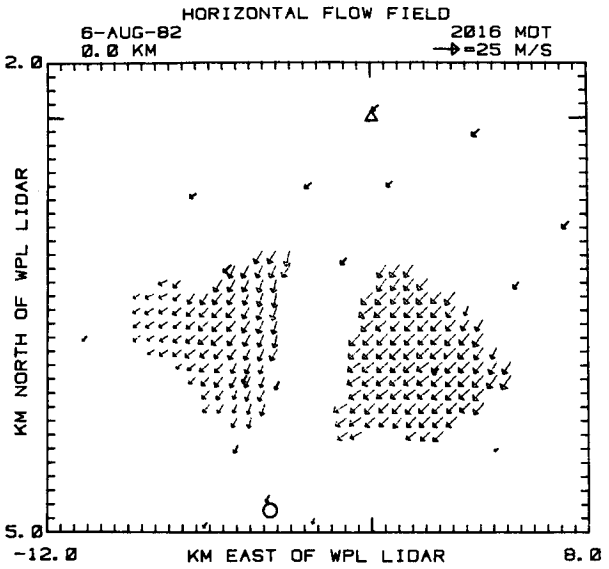

FIG. 3. Three-minute averaged wind field as measured by PAM network from 2015 to 2017 (solid arrows), superimposed on dual-Doppler lidar analysis of horizontal winds near surface (open arrows) at 2016 MDT, 6 August 1982. Circle and triangle mark positions of MSFC and NOAA/WPL lidars, respectively. Figure shows flow behind gust front which passed MSFC lidar at 2007 MDT.

encouraging to note the consistency of the present findings with those from previous studies of Great Plains thunderstorm outflows (e.g., Goff, 1976 and Charba, 1974), particularly regarding the weakening of the horizontal winds with height. Moreover, it was possible to corroborate an expression (Goff, 1976) that predicts the maximum low-level wind gust s in the cold air (which generally occurs shortly after frontal passage), given the gust front speed c:

$$s = 1.5c.$$

Goff found this expression to give an average absolute error of 1.2 m s^{-1} for the cases considered. In the present study, the observed gust-front speed of 11 m s^{-1} yields a prediction of 16 m s^{-1}, compared to the calculated maximum speeds near the surface of 15 m s^{-1} in the two dual Doppler analyses.

b. 15 July dual analysis

From 1730 to 1805 (times approximate) on 15 July 1982 a gust front associated with a virga line moved east-southeast through the JAWS network. Although the gust-front boundary was poorly defined, velocities as strong as 15.5 m s^{-1} within the outflow were reported by at least one PAM station. A dual analysis was made which included scans from 4 to 6 deg elevation at approximately 1759. Other low-elevation scans were too far removed in time to be considered for use. The gust front passed the MSFC lidar at roughly 1740, based upon a review of the PAM data. As in the above analysis, the region of overlapping scans was within the outflow. No precipitation was reported between the lidars. The reflectivity and radial velocity fields measured by CP-4 did not reveal a distinct frontal boundary. The PAM data indicated a temperature drop across the front of only 1 K or less. The MSFC and WPL lidars commenced scanning at 1748 and 1751, respectively, providing a more limited history of the outflow. A comparison between the MSFC lidar and CP-4 radial velocity returns was not feasible because of a lack of scans at similar times and differing elevation and azimuth angles.

The vertical extent of the volume scanned was smaller than the previous analysis; therefore, the first level at which horizontal winds were analyzed was set at 0.4 km above the surface. The dimensions of the computational volume were reduced to 14.5 × 14.5 × 1.0 km. The horizontal and vertical grid increment was 0.5 km. Figure 5 shows the 2 min averaged wind field as measured by the PAM network from 1758 to 1759, superimposed on the dual analysis at ~1759. The difference in direction between derived and observed winds amounts to 10 deg or less. At 0.9 km the horizontal flow field is nearly identical to that at 0.4 km, although with slightly stronger speeds (range 8–17 m s^{-1}) in the extreme western portion of the analysis.

c. 6 August lidar–radar comparison

Quantitative wind measurement comparisons between lidar and radar are rare. The JAWS project provided a unique opportunity to do collocated com-

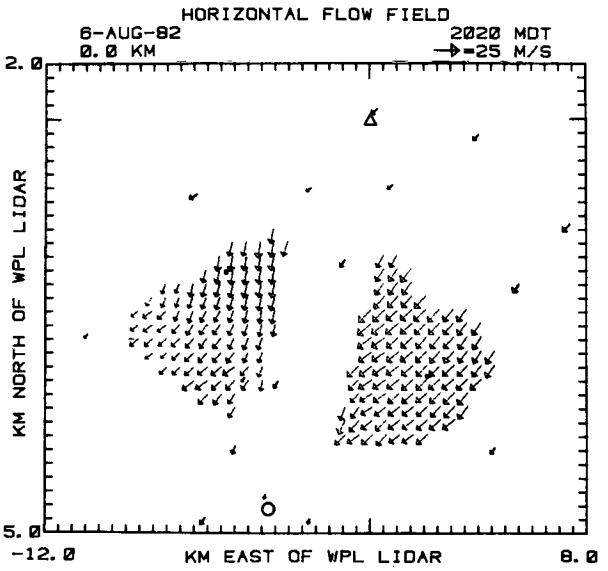

FIG. 4. As in Fig. 3, except PAM wind field measured during 2019–2021, superimposed on lidar-derived winds at 2020 MDT.

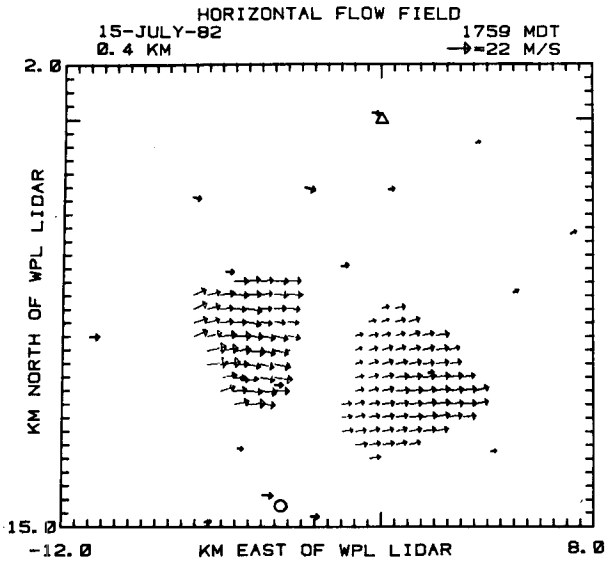

FIG. 5. As in Fig. 3, except 2-minute averaged PAM wind field measured during 1758–1759, superimposed on lidar-derived winds at 1759 MDT 15 July 1982. Figure shows flow behind gust front associated with virga line.

parisons between the two measurement systems. Hardesty *et al.* (1983) compared radial velocity measurements behind the 6 August 1982 gust front, described in Section 5a, using data from the WPL lidar and the NCAR CP-3 radar (with characteristics similar to CP-4). An rms difference of 2.8 m s^{-1} was found, which was attributed in part to collecting the two data sets at slightly different times and elevation angles. Moreover, the sampling volumes were different which, in the turbulent region behind the front, could easily give rise to comparable differences. More significantly, it was found that the mean of the radar measurement set was 2.1 m s^{-1} lower than that of the lidar. Since the WPL lidar values could have had a bias of up to 1 m s^{-1}, a minimum of 1.1 m s^{-1} of bias remained to be accounted for. They concluded that the bias is probably due to contamination of the radar velocity estimates by ground clutter, since overall radar signal levels were marginal over parts of the comparison volume.

A similar comparison has been made between the MSFC lidar and the NCAR CP-4 radar for a pair of scans on 6 August. Figures 6a and b represent the radial velocity distributions measured by the MSFC lidar and CP-4, respectively, at an elevation of 4 deg and separated by approximately 3 min. Both measurement sets were edited to remove data with low SNR; radar data obviously contaminated by ground clutter were also eliminated. The data were then interpolated to a horizontal grid with 0.5 km increment. Overlap existed over a 130 km^2 region. The general patterns are similar; both indicate a core of maximum horizontal winds within the outflow. Figures 6c and d show, respectively, the difference between the interpolated radar and lidar radial velocity values and the corresponding height contours taken from a topographic map. The height contours are basically northeast to southwest, which by coincidence roughly parallel the wind direction. The weakest radial winds and the smallest velocity differences are located to the northwest and southeast. To the north and northeast, where the terrain is of similar height or lower, smaller velocity differences occur ($\leqslant$2 m s^{-1}), as opposed to the east ($\leqslant$4 m s^{-1}) and south ($\leqslant$8 m s^{-1}), where the terrain is higher. Interestingly to the south-southwest a region occurs where the velocity difference isopleths are coincident with an elongated hill (note the 1645.9 m height contour).

It is important to note that the NCAR radar signal processors have the characteristic that when the Doppler velocity spectra are bimodal (one spectrum near zero associated with ground return and another offset from zero associated with meteorological return) the velocity of the stronger mode is captured, especially for signals greater than −95 dBm (Frush, 1981). Thus the estimated radial velocity is either close to zero, corresponding to the clutter, or close to the velocity of the meteorological signal without significant bias toward zero, provided the meteorological strength exceeds the clutter signal strength by more than ~6 dB (Frush, 1981). The CP-4 radar reflectivities over the analysis region averaged only about −105 dBm, however, corroborating the evidence presented above that the radar velocity estimates could have been affected by ground clutter contamination. A region of strong differences to the west ($\leqslant$8 m s^{-1}) is apparently not strongly associated with elevated terrain, and may instead be due more to reasons cited by the Hardesty *et al.* (1983) analysis, particularly to advective changes within the 3 minute period between observations. Figure 7 summarizes the information in Fig. 6c in the form of a scatter diagram. The scatter is large, with differences ranging from 4 to −9 m s^{-1} with respect to the lidar. The rms difference is 3.1 m s^{-1}, which could be accounted for by reasons cited above. However, the mean of the radar data set was 1.0 m s^{-1} lower than that of the lidar, comparable to that inferred by Hardesty *et al.* (1983). Trends in the scatter above and below the reference line indicate that the absolute value of the radar velocity estimate was biased toward zero. The average absolute difference is 2.3 m s^{-1}, which is comparable to the value of 2.1 m s^{-1} obtained by Hardesty *et al.*, since the velocities in their region of interest were all of one sign. This comparison, of course, is based on the assumption that the WPL measurement set contained a negligible bias. The height variations evident in Fig. 6d are comparable to those found in the region of the analysis cited above.

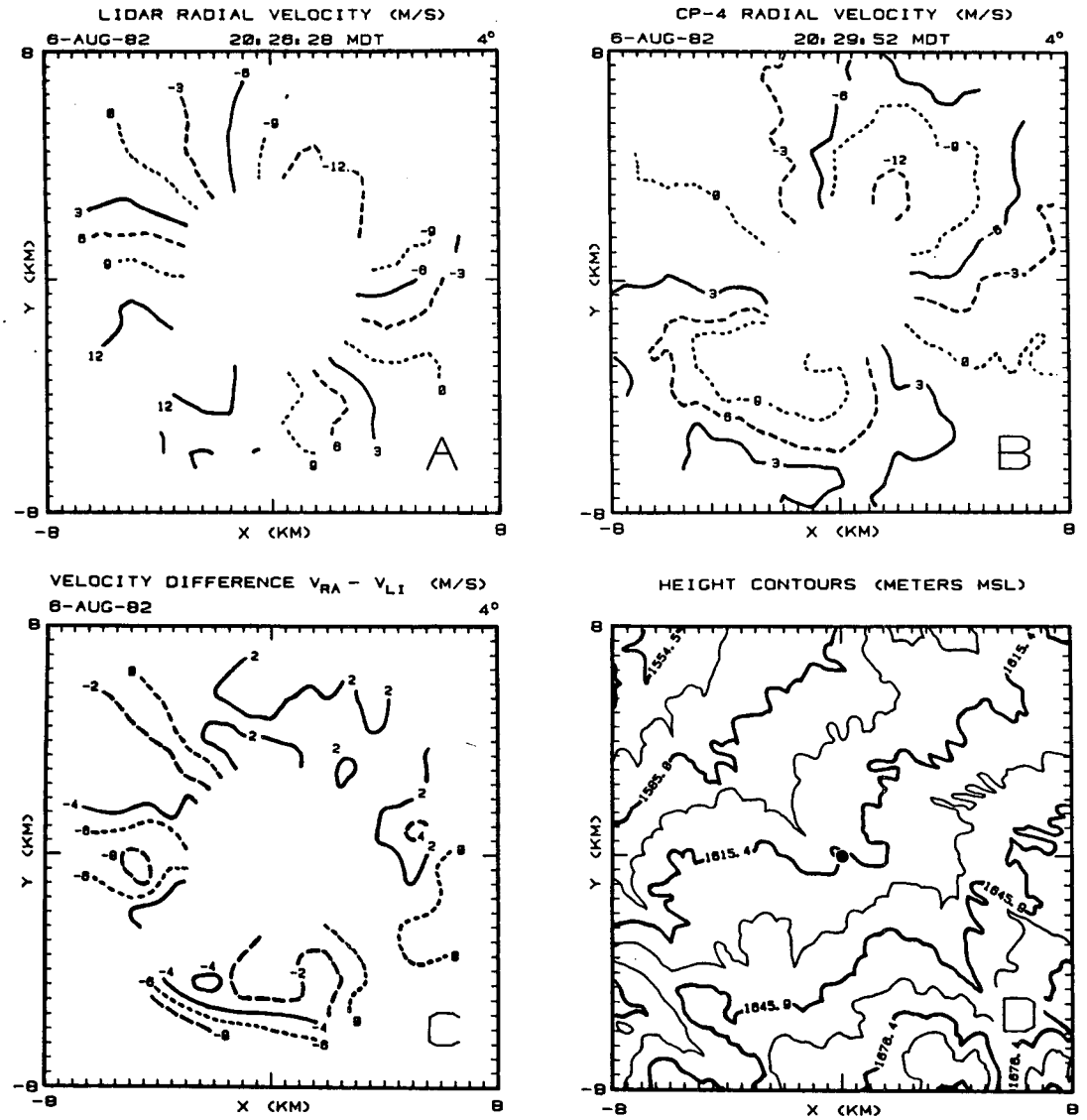

FIG. 6. (a) Radial velocity distribution as measured by MSFC lidar at 4 deg elevation on 6 August 1982. Measurement set has been edited. Data-void sector to the southwest is due to an obstruction. (b) As in (a) except for NCAR CP-4 radar. (c) Difference between interpolated lidar and radar radial velocities shown in (a) and (b), respectively. (d) Corresponding height contours taken from a topographic map. Dot marks position of lidar and radar.

Insufficient data exist from CP-4 radar and the lidar to objectively assess differences between the radar and the lidar analysis caused by the 3.5 min time separation. At 2026 the gust front was well out of range of the lidar, while at 2029 the gust front had advected out of the radar analysis domain.

As described in Section 2, the MSFC lidar data could have also contained a bias, with magnitude less than 1 m s^{-1}. It is not possible to remove such a bias during postprocessing. By training the lidar beam on hard targets in studies subsequent to participation in JAWS, the bias was found to exhibit a slow time dependence. Using the lidar data set from the above comparison, a combined measure of the bias and the effect of divergence was found by calculating the average radial velocity around a circle of radius $\sim$ 6 km. A value of 0.1 m s^{-1} was found which, using Eq. (3) from Caton (1963), corresponds to a divergence of $\sim 3 \times 10^{-5}$ s^{-1}, a reasonable value. Since it is unlikely that the effect of a strong actual divergence well behind the gust front could have approximately balanced a correspondingly large bias in the data, the small calculated divergence is considered evidence that on this occasion the magnitude of

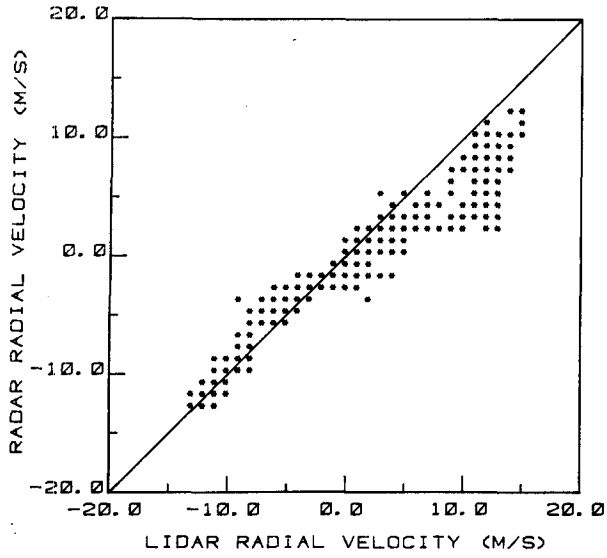

FIG. 7. Scatter diagram of MSFC lidar versus NCAR CP-4 radar radial velocity estimates. Performance characteristics of the two sensors suggest that ground clutter contamination biased radar estimates toward zero, hence the trend in scatter above and below reference line.

the bias was much smaller than 1 m s^{-1}. In addition, by using MSFC lidar data at 1 deg elevation at 2002, a divergence of -3×10^{-3} s^{-1} was calculated across an imaginary radial line perpendicular to and spanning the gust front. The value thus obtained is reasonable in the vicinity of the front; it is not susceptible to the effect of bias.

6. Summary and conclusions

The present study has conclusively demonstrated the feasibility of dual-Doppler analyses of winds using lidar measurements. Both sets of analyses (6 August and 15 July) involved flow behind gust fronts, which were consistent with surface wind measurements made by the NCAR Portable Automated Mesonet. The present study has served to reemphasize the validity of the Doppler lidar as a tool for studying boundary layer phenomena.

The present study has also pointed out differences between radar and lidar performance characteristics. The susceptibility of the lidar beam to attenuation by water vapor and thick clouds remains a serious disadvantage; unquestionably the radar is the instrument of choice for studying the dynamics within convective storms. On the other hand the second disadvantage, limited range, is not necessarily an insurmountable one. With the incorporation of new, more powerful lasers into lidar systems in general, as well as operation at nonabsorbing wavelengths, a significant increase in range will be forthcoming. A new laser is to be incorporated into the Wave Propagation Laboratory system, increasing transmitted power by a factor of 100. This modification should increase maximum range to more than 25 km (Hardesty *et al.*, 1983). At the Marshall Space Flight Center studies are under way wherein range has been extended by increasing the pulse duration, thereby increasing the output power.

A section was devoted to a comparison between the MSFC lidar and the NCAR CP-4 radar. As in the study by Hardesty *et al.*, a bias of 1–2 m s^{-1} was found in the radar data set, which could be explained by ground clutter contamination influencing the radar. Since the beamwidth of the lidar is almost 3 orders of magnitude smaller, it can scan arbitrarily close to the surface without susceptibility to bias by clutter. A further consequence of much narrower beamwidth is that less ambiguous velocity estimates can be obtained within localized regions of strong wind shear, particularly when scanning at low elevation angles. This feature, in addition to the advantage of the lidar relying on naturally occurring aerosols to obtain useable returns, suggests that the lidar is well suited for study of the dynamics in regions external to storms and, in general, to situations where returns due to insects or refractive index variations may not necessarily be representative of the air motion (for reasons cited in Section 3).

Analysis continues on the lidar data sets collected during JAWS. An obvious, yet significant finding has been that data analysis techniques [as well as computer software packages (see Oye and Carbone, 1981)] originally developed for radar are readily applicable to lidar. Finally, an important and perhaps more subtle result of the participation of Doppler lidar in JAWS is the field experience gained that would allow subsequent field programs to be pursued even more successfully.

Acknowledgments. The data analysis was performed on the NCAR Research Data Support System (RDSS) VAX 11/780. One of us (J.R.) would like to thank C. Mueller and R. Oye (NCAR) for instruction and guidance on the use of the RDSS. The dual Doppler analysis program was originally developed at the National Severe Storms Laboratory in Norman, Oklahoma, by P. S. Ray and C. Ziegler. One of us (C.K.) modified and implemented the program at NCAR. We gratefully acknowledge the discussions and suggestions rendered by J. W. Wilson and R. J. Keeler (NCAR), R. M. Hardesty and F. F. Hall (NOAA/WPL) and D. E. Fitzjarrald and W. W. Vaughan (NASA/MSFC). We also acknowledge M. Jackson (NOAA/WPL), who assisted in the identification of lidar data sets appropriate for analysis and who also provided plots of PAM wind fields.

JAWS is funded partially by NCAR; the National Science Foundation; the FAA, through Interagency

Agreement DTFA01-82-Y-10513; NASA, through Interagency Agreement H-59314B; and NOAA, through a cooperative agreement with the Program for Regional Observing and Forecasting Services of NOAAs Environmental Research Laboratory. This research was partially supported by the Universities Space Research Association under NASA Contract NAS8-34010.

REFERENCES

Atlas, D., 1964: Advances in radar meteorology. *Advances in Geophysics,* Vol. 10, Academic Press, 318–478.

Bilbro, J. W., G. H. Fichtl, D. E. Fitzjarrald, M. Krause and R. Lee, 1984: Airborne Doppler lidar wind field measurements. *Bull. Amer. Meteor. Soc.,* **65,** 348–359.

Caton, P. G. F., 1963: The measurement of wind and convergence by doppler radar. *Preprints, 10th Radar Meteorology Conf.,* Washington, DC, Amer. Meteor. Soc., 290–296.

Charba, J., 1974: Application of gravity current model to analysis of squall-line gust front. *Mon. Wea. Rev.,* **102,** 140–156.

Cressman, G. P., 1959: An operational objective analysis system. *Mon. Wea. Rev.,* **87,** 367–374.

Doviak, R. J., and C. T. Jobson, 1979: Dual doppler radar observations of clear air wind perturbations in the planetary boundary layer. *J. Geophys. Res.,* **84,** 697–702.

Eastwood, E., 1967: Radar Ornithology. Methuen, 278 pp.

Fowler, M. S., and A. H. LaGrone, 1969: Comparison of insect's flight characteristics with observed characteristics of radar dot angels. *J. Appl. Meteor.,* **8,** 122–127.

Frush, C., 1981: Doppler signal processing using IF limiting. *Preprints, 20th Radar Meteorology Conf.,* Boston, Amer. Meteor. Soc., 332–337.

Goff, R. C., 1976: Vertical structure of thunderstorm outflows. *Mon. Wea. Rev.,* **104,** 1429–1440.

Hardesty, R. M., K. Elmore and M. E. Jackson, 1983: Comparisons of lidar and radar wind measurements made during the JAWS experiment. *Preprints, 21st Radar Meteorology Conf.,* Edmonton, Alta., Amer. Meteor. Soc., 584–589.

Hardy, K. R., and H. Ottersten, 1969: Radar investigation of convective patterns in the clear atmosphere. *J. Atmos. Sci.,* **26,** 666–672.

Harper, W. G., 1958: Detection of bird migration by centimetric radar: A cause of radar angels. *Proc. Roy. Soc. London,* **B149,** 484–502.

Lee, R. W., and K. A. Lee, 1980: A poly-pulse pair signal processor for coherent Doppler lidar. *Tech. Digest, Coherent Laser Radar for Atmos. Sensing,* Aspen, Optical Soc. Amer.

McCarthy, J., J. W. Wilson and T. T. Fujita, 1982: The Joint Airport Weather Studies Project. *Bull. Amer. Meteor. Soc.,* **63,** 15–22.

——, R. Roberts and W. Schreiber, 1983: JAWS data collection analysis highlights, and microburst statistics. *Preprints, 21st Radar Meteorology Conf.,* Edmonton, Alta., Amer. Meteor. Soc., 596–601.

Oye, R., and R. Carbone, 1981: Interactive Doppler editing software. *Preprints, 20th Radar Meteorology Conf.,* Boston, Amer. Meteor. Soc., 683–689.

Post, M. J., R. A. Richter, T. R. Lawrence and F. F. Hall, 1981: National Oceanic and Atmospheric Administration pulsed coherent infrared Doppler lidar—Characteristics and data. *Proc. Soc. Photo-Opt. Instrum. Eng. Tech. Symp. West,* San Diego, SPIE, **300,** 60–65.

Ray, P. S., K. K. Wagner, K. W. Johnson, J. J. Stephens, W. C. Bumgarner and E. A. Mueller, 1978: Triple-Doppler observations of a convective storm. *J. Appl. Meteor.,* **17,** 1201–1212.

——, C. L. Ziegler and W. Bumgarner, 1980: Single- and multiple-Doppler radar observations of tornadic storms. *Mon. Wea. Rev.,* **108,** 1607–1625.

Wilson, J., R. Carbone, H. Baynton and R. Serafin, 1980: Operational application of meteorological Doppler radar. *Bull. Amer. Meteor. Soc.,* **61,** 1154–1168.